Comparative Study of Interactive Seed Generation for Growcut-Based Fast 3D MRI Segmentation

Toshihiko Yamasaki[1,2], Tsuhan Chen[2], Masakazu Yagi[3], Toshinori Hirai[4], and Ryuji Murakami[4]

[1]The University of Tokyo, Tokyo, Japan, [2]Cornell University, Ithaca, United States,
[3]Oaska University, Osaka, Japan, [4]Kumamoto University, Kumamoto, Japan
E-mail: yamasaki@hal.t.u-tokyo.ac.jp, ty273@cornell.edu

***Abstract*— This paper proposes a speed-enhanced growcut method and presents comparative study of seed setting methods for fast 3D medical image (MRI) segmentation. The processing time tends to be larger in 3D image segmentation because of the large number of neighboring voxels as well as the number of voxels themselves. In this paper, two seed setting methods are proposed for our fast growcut-based segmentation algorithm: sphere-based bounding box method and label transfer based method using SIFT flow. Experimental results demonstrate that the tumor segmentation for each patient can be done very quickly as compared to the previous works. The segmentation accuracy can also be made very high with only a few user interactions.**

I. INTRODUCTION

Medical image segmentation is one of the most important but yet difficult processing problems for the pathological diagnosis. It also plays an important role in computer-aided diagnosis systems. In addition to a number of image segmentation algorithms aiming at natural images [1]-[3], there are also algorithms dedicatedly designed for medical images [4]-[10]. Medical images have their own unique properties and are different from natural scene images. For instance, they tend to have more bit levels (12-16 bits), images are gray-scale, and structure and appearance of the objects is not always clear.

3D volumetric analysis, in particular, is important for radiation therapy and follow-up observation. In fact, the number of slices of MRIs for each patient is increasing with the advancement of the equipments. Besides, chances for us to take MRIs are also increasing because MRI inspection is being included medical checkups. Because of these reasons, the number of MRIs that medical doctors have to observe is increasing a lot. As a result, efficient segmentation tool is highly demanded. However, most of medical image segmentation algorithms presented so far focus on each 2D image slice [4] or 3D images with lower resolution [5]-[8] because of the computational complexity. The computational time is increased not only by the number of image slices in the z direction but also by the number of neighboring voxels in the 3D space. The number of the neighboring pixels in 2D images is eight (3^2-1), but that in 3D images is 26 (3^3-1).

In our previous work [11], we proposed a fast growcut-based 3D tumor segmentation algorithm. The processing time was drastically reduced by truncating unnecessary process based on the confidence of the label for each voxel. In order to have the algorithm work efficiently, proper seed setting in the 3D image space is an important issue. Therefore, in this paper, comparative study for label seed setting is conducted using a sphere-based bounding box method and label transfer based method. The experimental results show that the two proposed approaches effectively help users to get better segmentation results as compared to conventional scribbling. It is also shown that the segmentation results converge with only a few user interactions. The difference from our previous work [11] is that the whole system including user interaction interface to correct the errors is implemented and that two label seed setting is compared on the system.

The rest of this paper is organized as follows. Section 2 summarizes the truncation algorithm to omit unnecessary calculation for the growcut algorithm. In Section 3, the proposed interfaces for proper label seed setting are explained. The experimental results are demonstrated in Section 4 followed by concluding remarks in Section 5.

II. SPEED-ENHANCED GROWCUT ALGORITHM

The peudo-code of the speed enhanced growcut algorithm is shown Algorithm 1. Here, p is a voxel in a set of voxels P. q is the voxel in Moore neighborhood of the voxel p: $N(p)$. The label for the pixel p at the t-th stage is denoted as l_p^t and the strength of the voxel is denoted as s_p^t where the range for the s is set as [0,1] without loss of generality. In the initial stage, the strengths for the voxels whose seeds are assigned are set to one and those for the unknown voxels are set to zero. C_p is the luminance value of the voxel p. $g(x)$ is the monotonous function defined as

$$g(x)=1-\frac{x}{\max(C)} \tag{1}$$

The difference from the original growcut [3] is high-lightened by the bold-type fonts.

Growcut is one of the region-growing based segmentation algorithms. Labels assigned to the seeds iteratively penetrate to the neighboring voxels depending on the voxel value difference (lines 10-13). The strength of the label to penetrate into its neighbors is defined by the voxel value difference. The processing cost depends mainly on the number of voxels

Algorithm 1: Pseudo-code of the speed-enhanced 3D growcut algorithm. The difference from [3] is high-lightened by the bold type fonts.

```
01: while the labels are not converged
02:   // for each voxel
03:   for ∀p ∈ P
04:     // copy previous state
05:     l_p^{t+1} = l_p^t ;
06:     s_p^{t+1} = s_p^t ;
07:     // neighbors attack current cell
08:     if (for ∀s_q^t (q ∈ N(P)), s_q^t ≤ s_p^t)
09:       for ∀q ∈ N(P)
10:         if g(|C_p − C_q|) · s_q^t > s_p^t
11:           l_p^{t+1} = l_q^t ;
12:           s_p^{t+1} = g(|C_p − C_q|) · s_q^t
13:         end if
14:       end for
15:     end if
16:   end for
17: end while
```

to calculate because each voxel has to look at its 26 neighboring voxels every time of iteration. The skipping method contributes to reducing the number of voxels to calculate. If the confidence value of the present voxel is equal to or stronger than those in its neighboring voxels, there is no chance for the voxel label to be overwritten. This means, in such cases, the region growing process in lines 9-14 in Algorithm 1 can be skipped. Therefore, how to set the initial seeds, whose strength is one, affects the computational efficiency.

III. Label Seed Setting

The key for the truncation algorithm in Section 2 to work efficiently is to assign seeds to as many voxels as possible. On the other hand, assigning such seeds by scribbling every slice is not practical. For example, typical segmentation software we use requires tracing the boundary of the tumor every few slices. Although a magnetic lasso tool can help the user to scribble and boundaries can be interpolated to the other slices, the interaction time is still very huge.

In this section, two label seed setting methods are described. After the first segmentation is obtained, labels are refined by free-form scribbles in both cases.

A. Bounding Box By Sphere Based Setting

In our sphere-based bounding box method, users roughly specify the center of the tumor and two diameters. One diameter (red region in Fig. 1) is used to specify the positive seed region and the other diameter (blue region in Fig. 1) is

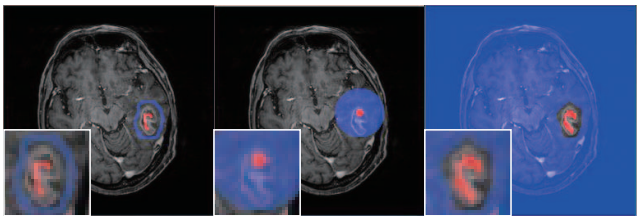

Fig. 1. Seed generation: (left) conventional scribbles, (middle) sphere-based bounding box method, (right) label transfer based method. Red voxels are positive seeds and blue voxels are negative seeds. For the bounding box by sphere, unknown region is blue and negative seeds are transparent.

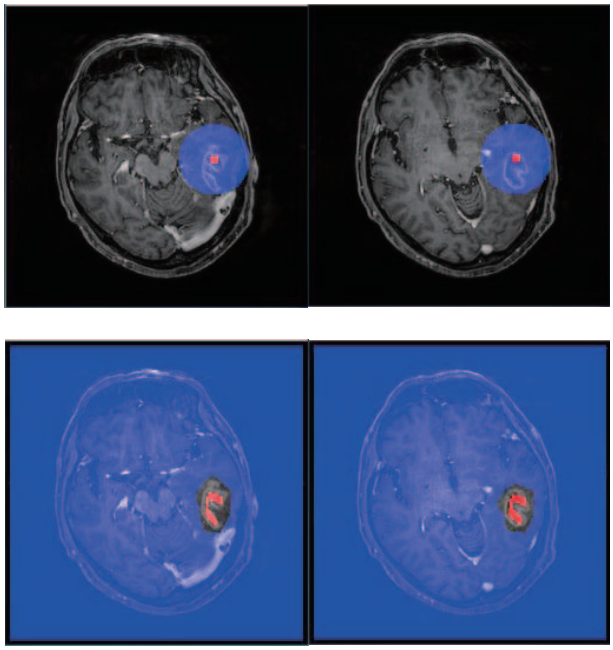

Fig. 2. Labels in other slices (plus and minus 3 slices from Fig. 1): (top) sphere-based bounding box method, (bottom) label transfer based method.

for unknown region. This method is based on an assumption that the shape of tumors are close to sphere. At least, one seed should be specified to each tumor. Two or more seeds can be added to increase the accuracy if needed. The black region where no seed was explicitly assigned is used as the negative seed. The required interaction is browsing the slices, clicking a point, and setting two diameters.

B. Label-Transfer Based Setting

Another possible solution is giving scribbles to only a single slice (or some slices) and transferring the seeds to the neighboring layers. For this purpose, a SIFT flow algorithm [12] is employed. The SIFT flow algorithm extracts the SIFT descriptors [13] for every pixels in a dense way and take the correspondents between the two images. Then, the label correspondence search is expressed as a discrete optimization problem:

$$E(\mathbf{w}) = \sum_{\mathbf{p}} \left\| s_1(\mathbf{p}) - s_2(\mathbf{p}+\mathbf{w}) \right\|_1 + \frac{1}{\sigma^2}\left(u^2(\mathbf{p}) + v^2(\mathbf{p})\right) + \sum_{(\mathbf{p},\mathbf{q})\in\varepsilon} \min\left(\alpha\left|u(\mathbf{p}) - u(\mathbf{q})\right|, d\right) + \min\left(\alpha\left|v(\mathbf{p}) - v(\mathbf{q})\right|, d\right) \quad (2)$$

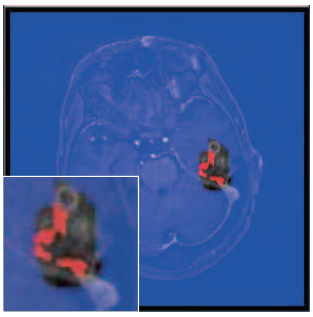

Fig. 3. Label transfer error in SIFT flow (10th slice from the first slice).

where $\mathbf{w}(\mathbf{p})=(u(\mathbf{p}), v(\mathbf{p}))$ is the displacement vector at pixel location $\mathbf{p}=(x, y)$, $s_i(\mathbf{p})$ is the SIFT descriptor extracted at location $\mathbf{p}$ in slice i and ε is the spatial neighborhood of a pixel. σ, α, and d are the control parameters and they are set as default. By using Eq. (2), the correspondence between the SIFT features between the slices are optimized and the labels in the current layer are transferred to the next layer depending on the extracted flow. Although the shape of the tumor changes a lot even between the neighboring slices, the correspondence is taken thanks to the high local feature description ability of the SIFT algorithm. And by considering the flow consistency with neighboring pixels, better correspondence is obtained than taking the correspondence pixel by pixel.

IV. Experimental Results

The experiments were conducted using 256 x 256 x 200 MRIs of 10 patients. The ground truth segmentation data were generated by scribbling each slice by hand by a doctor. The performance was evaluated using a Windows 7 laptop PC with Intel Core i7 M640 (2.80GHz) and 8GB memory. Two people participated in the evaluation. The segmentation was repeated until the users are satisfied with the results. In the first iteration, either of the two methods described in Section III was used for the seed generation. For the second and latter iterations, the users were required to give free-hand scribbles to refine the segmentation results in the previous stage. All the algorithms were implemented by using C++ except for the SIFT flow algorithm which was written in MATLAB [12].

The generated seed labels are shown in Fig. 1. The leftmost image was generated by conventional free-hand scribbles only to a single layer. The image in the middle is the result of the sphere-based bounding box method and the image on the right is generated by scribbles for label transfer-based method. It took 30s, 39s, 44s, respectively on average to draw such seeds. How the labels are transferred to the other slices is illustrated Fig. 2. It is shown that the label seeds assigned in the first slice (in Fig. 1) are successfully transferred. The label transfer based method failed in the slices where the tumor was vanishing. An example is shown in Fig. 3. Once proper correspondence is lost, label transfer also fails in the latter slices. In such a case, the errors are corrected by the user scribbles. On the other hand, in the sphere based bounding box method, such error does not happen.

Table 1. Average segmentation performance and processing time.

	Prec.	Recall	Time
Ground-truth	-	-	~3600s
Conventional scribbles (after the 1st iteration)	85%	76%	2389s
Bounding box by sphere (after 3 iterations)	92%	90%	251s
Label transfer by SIFT flow (after 3 iterations)	88%	92%	1019s

Table 2. Average processing time: (a) sphere-based bounding box method, (b) label transfer based method.

(a)

Operations	Time required
Draw sphere(s)	28.6s
Revise the seeds	6.8s
Run growcut	12.8s
Revise the results	186.4s
Run growcut	5.2s
Revise the results	5.8s
Run growcut	5.6s
Total	251s

(b)

Operations	Time required
Scribbling	33.8s
Run SIFT flow	597.8s
Revise the seeds	237.4s
Run growcut	8.6s
Revise the results	109s
Run growcut	4.4s
Revise the results	23.6s
Run growcut	4.4s
Total	1019s

Table 1 shows the segmentation accuracy and average processing time. When the conventional scribbling is used, only the accuracy after the first iteration is shown because the average recall rate was only 76% and a lot of scribbling to correct the errors was required, resulting in more efforts than making the ground truth. When the sphere-based bounding box was drawn, the precision and recall rates converged only with 251 seconds. Actually, the accuracy got saturated after the second iteration (at 240 seconds from the start). When the label transfer based method is employed, the accuracy is almost the same while demanding more processing time. 59% of the time (598 seconds) was consumed for calculating the flow by MATLAB, the processing cost would be decreased when the SIFT flow was implemented by low-level programming languages.

The details of the operations and time required for each step are summarized in Table 2. It can be observed that the proposed seed generation methods contribute to reducing the time for our speed-enhanced growcut algorithm. The

Table 3. Comparison of the processing time.

	Resolution	Time
[9]	256x256x124	430s
[10]	256x256x50	6600s
Proposed (bounding box)	256x256x200	240s (two iterations)

processing time for the first iteration was 13 seconds and 9 seconds, respectively while the baseline (simply scribbling in a single slice) took about 2,400 seconds. It is reasonable to ask the users to wait for about 10 seconds to have the segmentation done. In addition, it is shown that most of the time is used in user interaction. If the touch interface is available instead of using a mouse, it would reduce the time for user interaction.

The comparison with previous works is shown in Table 3. Even though the number of slices is larger, our proposed method is more efficient than the state-of-the-art approaches [9][10].

A typical precision and recall rates over time using a certain MRI set are shown in Fig. 4. The precision and recall rates are already high after the first iteration and get improved after revising the segmentation results and going through the second iteration. On the other hand, the third iteration does not contribute to improving the segmentation performance very much because the labels are not revised very much. The reason why the precision and recall does not go up to 100% is that the results by two subjects are slightly different from each other.

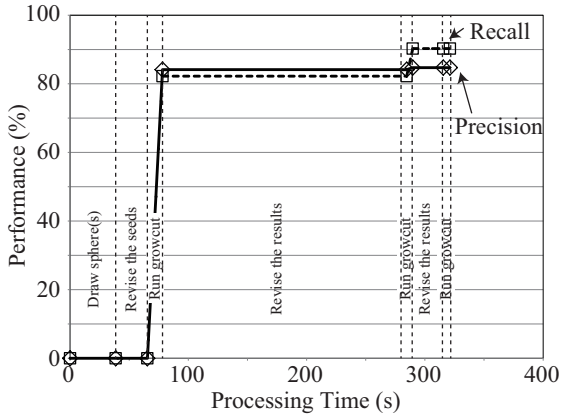

Fig. 4. Typical precision and recall rates over time using the bounding box approach.

V. Conclusions

In this paper, a speed-enhanced growcut system in conjunction with efficient label seed setting interface was presented. Both the sphere-based bounding box approach and label-transfer based approach demonstrated high segmentation performance and the total processing time was reduced to 7.0% and 28% (even with MATLAB implementation) of the baseline approach.

One of the remaining problems is an efficient scribbling interface. Super-pixelization/voxeliation would help the users to give scribbles easily, but the growcut algorithm itself should be extended so that graph structure can be considered.

Acknowledgment

T. Yamasaki is supported by the program of JSPS Postdoctoral Fellow for Research Abroad. The medical images have been sanctioned by the medical ethics board of Kumamoto University, Japan.

References

[1] Y. Boykov and M.-P. Jolly, "Interactive graph cuts for optimal boundary & region segmentation of objects in N-D images," Proc. IEEE ICCV, vol. I, pp. 105-112, 2001.

[2] C. Rother, V. Kolmogorov, and A. Blake, "GrabCut: interactive foreground extraction using iterated graph cuts," SIGGRAPH'04, pp. 309-314, 2004.

[3] V. Vezhnevets and V. Konouchine, "`Grow-Cut' - interactive multi-label N-D image segmentation," Proc. Graphicon, pp. 150-156, 2005.

[4] A. Capelle, O. Alata, C. Fernandez, S. Lefevre, and J. Ferrie, "Unsupervised segmentation for automatic detection of brain tumors in MRI," Proc. ICIP, pp. 613-616, 2000.

[5] X. Xuan and Q. Liao, "Statistical structure analysis in mri brain tumor segmentation," Proc. Fourth International Conference on Image and Graphics, pp. 421–426, 2007.

[6] F. Nicolier, S. Lebonvallet, E. Baudrier, and S. Ruan, "Hausdorff distance based 3D quantification of brain tumor evolution from MRI images," Proc. IEEE EMBS, pp. 5597–5600, 2007.

[7] N. Zhang, S. Ruan, S. Lebonvallet, Q. Liao, and Y. Zhu, "Multi-kernel SVM based classification for brain tumor segmentation of mri multi-sequence," Proc. IEEE ICIP, pp. 3373-3376, 2009.

[8] S. Ait-Aoudia, F. Belhadj, and A. Meraihi-Naimi, "Segmentation of volumetric medical data using hidden Markov random field model," Proc. International Conference on Signal-Image Technology & Internet-Based Systems, pp. 65–72, 2009.

[9] T. Wang, I. Cheng, and A. Basu, "Fully automatic brain tumor segmentation using a normalized Gaussian Bayesian classifier and 3D fluid vector flow," Proc. IEEE International Conference on Image Processing (ICIP), pp. 2553–2556, 2010.

[10] S. Ahmed, K. Iftekharuddin, and A. Vossough, "Efficacy of texture, shape, and intensity feature fusion for posterior-fossa tumor segmentation in MRI," IEEE TITB, vol.15, no.2, pp. 206–213, March 2011.

[11] T. Yamasaki, T. Chen, M. Yagi, Hirai, and Murakami, "Growcut-based fast tumor segmentation for 3D magnetic resonance images" SPIE Medical Imaging, 2012.

[12] C. Liu, J. Yuen, A. Torralba, J. Sivic, and W. T. Freeman, "SIFT flow: dense correspondence across different scenes," Proc. ECCV, Part III, LNCS 5304, pp. 28-42, 2008.

[13] D. Lowe, "Distinctive image features from scale-invariant keypoints," IJCV, 60(2), pp. 91-110, 2004.